Colloid & Polymer Science Colloid Polym Sci 272:121–129 (1994)

Phase separation in blends of two homopolymers and a diblock copolymer during film casting

B. Löwenhaupt and G. P. Hellmann

Deutsches Kunststoff-Institut, Darmstadt, FRG

Abstract: Demixing during film casting of blends of polystyrene, polymethylmethacrylate, and a symmetric diblock copolymer of styrene and methylmethacrylate is discussed. The concentration fluctuations in the homogeneous solutions were calculated in mean field approximation. The structures in the homogeneous and demixed solutions and in the dry films were measured by small-angle x-ray scattering, and the morphologies of the dry films were characterized by transmission electron microscopy. The structure of the dry blends is evidently already pre-formed in solution.

Key words: Polymer blends – block copolymers – phase morphologies

Introduction

Block copolymers $\alpha\beta$, with two immiscible blocks α and β, can refine and stabilize the phase morphologies of polymer blends A/B of two immiscible homopolymers A and B. This "compatibilizer effect" [1–4] of copolymers $\alpha\beta$ is believed to be rooted in their ability to form microphase morphologies [5, 6] that are thermodynamically stable (Fig. 1). The copolymer chains $\alpha\beta$ stabilize the thermodynamically unstable macrophase morphologies of the blends A/B [7] by covering the interfaces in monomolecular layers, as is illustrated by Fig. 2.

However, block copolymers are often not as efficient as desired, because their chains have two other options, besides covering interfaces. The chains $\alpha\beta$ can i) form micelles inside the phases of A and B [8–12], or ii) form macrophase domains of their own [13–18]. In blends where, chemically, A equals α and B equals β, the ratio

$$\lambda = V_H/V_{\alpha\beta}, \quad V_H = V_A = V_B \tag{1}$$

of the chain volumes (i.e., the molecular weights over the densities) controls the morphologies [7, 19, 20]. At $\lambda \geq 1$, where the homopolymer chains A and B are longer, $\alpha\beta$ forms macrophases like a third, immiscible homopolymer, as is discussed in ref. [19]. At lower λ, $\alpha\beta$ forms micelles as well as interface layers as indicated in Fig. 2. This situation is discussed in ref. [20] and is considered again, below.

Phase separation during solvent evaporation was studied, in solutions of blends of polystyrene (PS) and polymethylmethacrylate (PMMA), of equal chain volumes and present in equal amounts, and of a longer-chained symmetric diblock copolymer P(S-b-MMA), which was added in various amounts. The experiments started in homogeneous solutions, with toluene as a non-selective solvent.

The question was, how much of the copolymer would be needed to convert the coarse macrophase morphologies produced by the blend PS/PMMA into fine microphase structures resembling those of the copolymer P(S-b-MMA) (Fig. 1). In other words, the question was how good a compatibilizer the copolymer was. Three techniques were employed to analyze the solutions during solvent evaporation (i.e., during film casting) as well as the dry films (Fig. 3):

- The concentration fluctuations in the still homogeneous solutions were calculated using the random phase approximation (RPA).

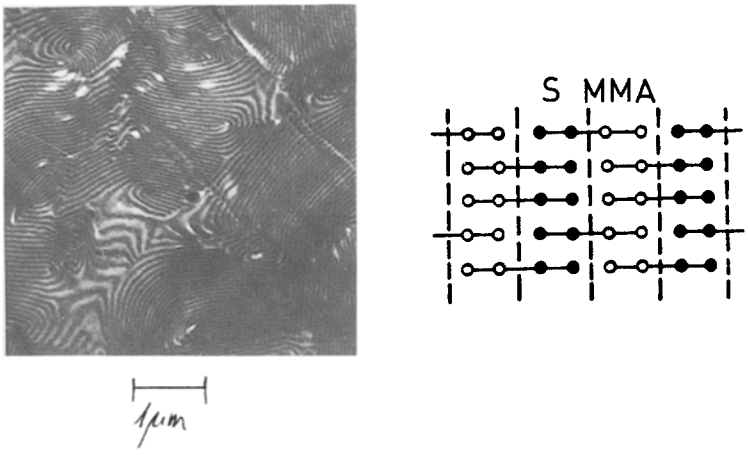

Fig. 1. TEM and schematic phase structure of the diblock copolymer P(S-b-MMA)-I

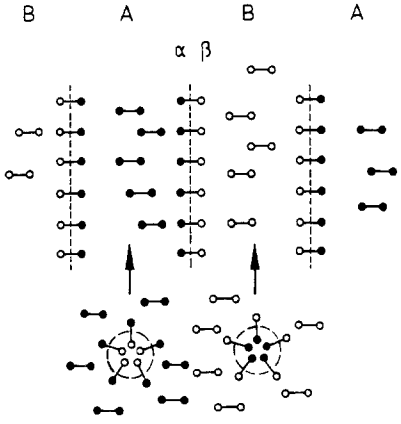

Fig. 2. Schematic phase structure of a blend $A/B/\alpha\beta$ of two homopolymers A and B and a diblock copolymer $\alpha\beta$, with copolymer chains in interfaces and in micelles

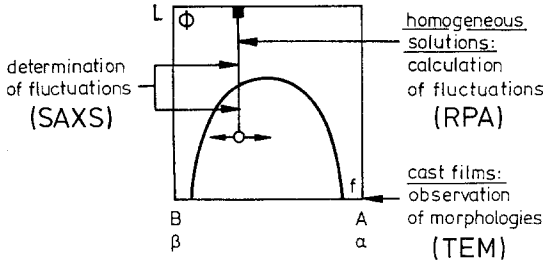

Fig. 3. Phase diagram of solutions $A/B/L$ or $\alpha\beta/L$ (L: solvent) with a miscibility gap. The ranges where RPA, SAXS, and TEM yield informations are indicated

- These fluctuations and the phase structures in the demixed solutions and films were measured using small-angle x-ray scattering (SAXS).
- The morphologies of the dry films were characterized using transmission electron microscopy (TEM).

The assumption was tested that *the morphologies found in the dry films are preformed in the solutions prior to phase separation*, so that the blend morphologies can be predicted by RPA calculations.

Short-chained homopolymers were chosen to ensure $\lambda < 1$. This rules out that the copolymer separates off in macrodomains [19]. In ref. [20], the copolymer P(S-b-MMA) had five times the chain volume of the homopolymers. Those blends PS/PMMA/P(S-b-MMA) were well suited for TEM investigations, which were compared with the RPA predictions. This comparison was a bit indirect, RPA characterizing only the homogeneous solutions and TEM only the dry blends. The method to close the gap is SAXS (Fig. 3), for which shorter copolymers are better suited. Below, an on-line SAXS study of the phase separation process in solution, during solvent evaporation, is presented that was performed on blends PS/PMMA/P(S-b-MMA) with a copolymer having only twice the chain volume of the homopolymers. The RPA model is outlined briefly, and TEM data are discussed at the end.

Experimental

The PS ($M_w = 32\,000$, $M_w/M_n = 1.9$) and the PMMA ($M_w = 35\,000$, $M_w/M_n = 2.0$) were made

by radical polymerization, the diblock copolymers P(S-b-MMA)-I ($M_w = 187\,000$, $M_w/M_n = 1.04$) and P(S-b-MMA)-II ($M_w = 66\,000$, $M_w/M_n = 1.04$), both with blocks of equal molecular weight, were made by Polymer Standards Service (PSS, Mainz, Germany) by anionic polymerization. For film casting and TEM see ref. [19]. SAXS curves were measured using a Kratky-Kompakt-Kleinwinkel-system (A. Paar, Graz, Austria) with a position sensitive detector, on packs of films or on solutions. During solvent evaporation, the x-ray beam was guided through a cuvette of 2-mm thickness, just above the bottom. The curves were desmeared and Lorentz-corrected. The solvent evaporation time was converted into the solvent concentration by calibration.

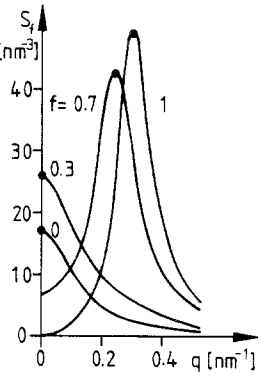

Fig. 4. Structure factors S_f of homogeneous solutions $[(PMMA/PS)_{1-f}/P(S\text{-b-}MMA)\text{-}II_f]_{1-\phi}/toluene_\phi$, of different copolymer contents f, calculated for the toluene concentration $\phi = (\phi^* + 0.05)$ (compare Fig. 8), ●: maximum at the characteristic wave vector q^*

RPA model calculations

The random phase (or mean field) approximation (RPA) model for concentration fluctuations in multicomponent systems [19–22] as well as RPA calculations for homogeneous blend solutions $A/B/\alpha\beta/L$, in particular of the solutions PS/PMMA/P(S-b-MMA)-I/toluene, were treated at length in refs. [19, 20]. Only the relevant ideas, relating to phase separation during solvent evaporation, are repeated.

The solutions have five components, the chains A and B, the blocks α and β, and the molecules of the solvent L. Calculated are structure factors S_{ij} characterizing the correlated fluctuations of these components, on all wave vector scales q. The S_{ij} depend on form factors S_i describing the intramolecular correlations of the components, and on parameters χ_{ij} describing the intermolecular interactions between the components. Each S_i depends on the volume fraction as well as on the chain volume and the shape of the molecules of one component.

The solutions PS/PMMA/P(S-b-MMA)/toluene are comparatively simple systems. The variables are (for the constant parameters see ref. [20]):

- the volume fractions ϕ of L (in the solutions) and f of $\alpha\beta$ (in the dry blends), and
- the chain volumes $V_{\alpha\beta}$ of $\alpha\beta$ and V_H of A and B, the latter being given in terms of the chain volume ratio λ (Eq. (1)).

Of interest is the structure factor

$$S_f = S_{AA} + S_{\alpha\alpha} + 2S_{A\alpha} = S_{BB} + S_{\beta\beta} + 2S_{B\beta}\,, \tag{2}$$

which describes the fluctuations of the polymeric components. The solvent L is nonselective and serves only as a diluent that homogenizes the blends.

Structure factors S_f are shown in Fig. 4, for homogeneous solutions of the blend PS/PMMA, the copolymer P(S-b-MMA)-II, and two blends PS/PMMA/P(S-b-MMA)-II. The fluctuations at the maximum of S_f dominate the structure of the (still homogeneous) solutions. The height of the maximum is not important, but rather its position at the *characteristic wave vector* q^*. The assumption to be tested below is that, when the solutions phase separate during solvent evaporation, phase structures will be formed on a scale similar to q^*.

Characteristic for homopolymer blends A/B ($f = 0$ in Fig. 4) is $q^* \to 0$, meaning that macroscopic fluctuations are most stable, while $q^* > 0$ is characteristic for copolymers $\alpha\beta$ ($f = 1$ in Fig. 4), meaning that fluctuations on a microscopic (in fact even submicroscopic) scale are stable. For ternary blends $A/B/\alpha\beta$, a transition concentration f^* of the copolymer exists where $q^* \to 0$ changes to $q^* > 0$. According to the above assumption, *this concentration f^* is a measure of the quality of $\alpha\beta$ as a compatibilizer for the blend A/B*. Since macrophase morphologies are expected at $f < f^*$ and microphase morphologies at

$f > f^*$, a good compatibilizer is distinguished by a low f^*.

As the solvent is evaporated, the structure factor S_f grows until its maximum diverges at the critical solvent concentration ϕ^*:

$$S(q^*, \phi^*) \to \infty \; . \tag{3}$$

This condition yields model phase diagrams $\phi^*(f)$ of the solutions.

The structure factor S_f and, thereby, the characteristic wave vector q^* and the critical solvent concentration ϕ^* can be measured by SAXS, while the coarseness $\zeta = 2\pi/q^*$ of morphologies can be determined by TEM.

SAXS curves

In Fig. 5, SAXS curves are shown that were measured during solvent evaporation, in solutions of the binary homopolymer blend PS/PMMA, the copolymer P(S-b-MMA)-II, and two ternary blends PS/PMMA/P(S-b-MMA)-II. The homopolymer chains are as long as the copolymer blocks ($\lambda = 0.50$).

The SAXS curves are of the types predicted by Fig. 4. The binary blend and the ternary blend with $f = 0.3$ yield decay curves ($q^* \to 0$) while the copolymer and the ternary blend with $f = 0.7$ yield peaks ($q^* > 0$). In Fig. 6, the measured characteristic wave vectors q^* are compared to the model. The structure coarseness ζ determined from TEM pictures is also shown, inverted by $q^* = 2\pi/\zeta$ (see next section). Not surprisingly, the model does not predict q^* exactly. But the model predicts a transition concentration at $f^* = 0.42$ and indeed microphase structures giving rise to a SAXS peak were observed only at $f > f^*$.

As long as the blend solutions of Fig. 5 are dilute and homogeneous, they hardly scatter

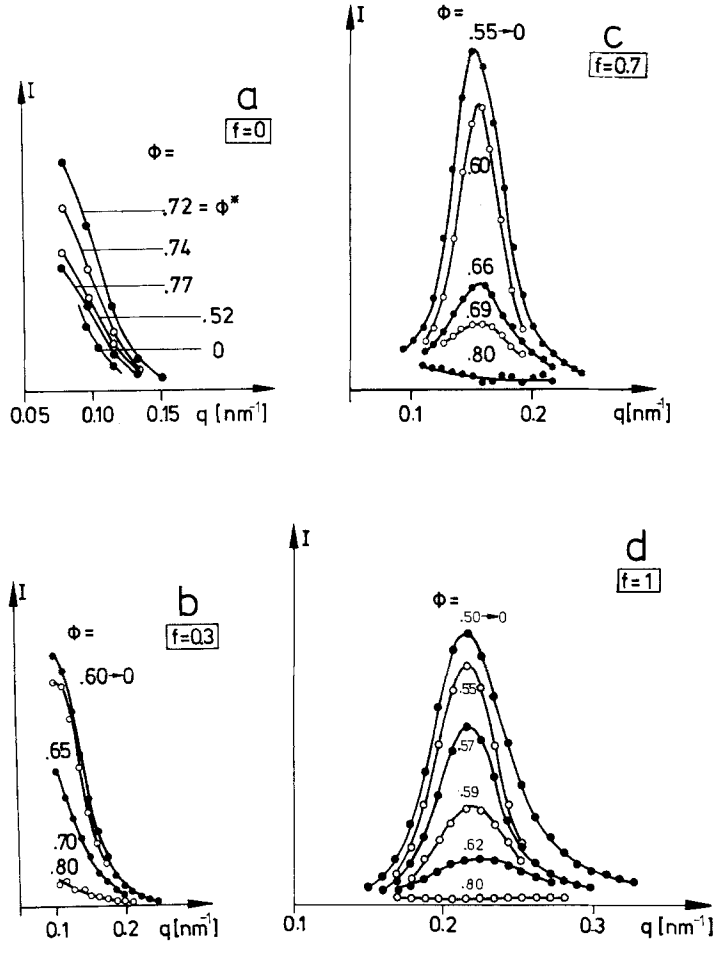

Fig. 5. SAXS curves of homogeneous and demixed solutions PMMA/PS/P(S-b-MMA)-II/toluene with a) $f = 0$ (no copolymer), b) $f = 0.3$, c) $f = 0.7$, d) $f = 1$ (only copolymer), measured during film casting at the indicated solvent concentration ϕ

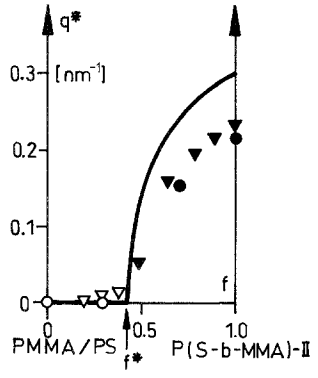

Fig. 6. Characteristic wave vector q^* of blends PMMA/PS/P(S-b-MMA)-II, f^*: transition concentration, ●: SAXS, ▼: TEM (symbols full: microphases, empty: macrophases), curve calculated

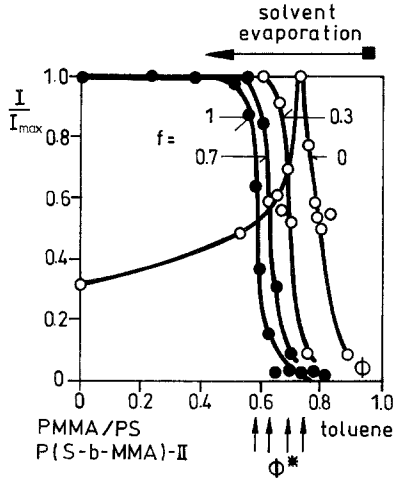

Fig. 7. Normalized SAXS intensity I at a constant q, during solvent evaporation (data from Fig. 5), $I = I(q = 0.1\ \mathrm{nm}^{-1})$ for $f = 0$ and $f = 0.3$ (Fig. 5a, b), $I = I(q^*)$ for $f = 0.7$ and $f = 1$ (Fig. 5c, d), ●: microphase, ○: macrophase separation, ϕ^*: critical solvent concentration (point of inflection or, for $f = 0$, maximum position)

x-rays. But as the solvent evaporates, the SAXS intensity increases rapidly to a maximum when demixing starts, as is shown in Fig. 7. This behavior corresponds approximately to the model prediction of Eq. (3) of a critical scattering near ϕ^*.

Figure 8 shows the calculated and measured phase diagram $\phi^*(f)$. Equation (3) predicts macrophase (at $f < f^*$) and microphase (at $f > f^*$)

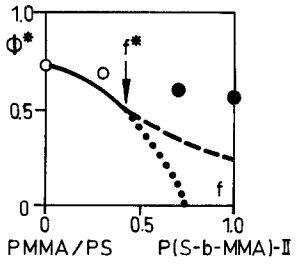

Fig. 8. Critical solvent concentration ϕ^* of the solutions PMMA/PS/P(S-b-MMA)-II/toluene, microphase (---, ●) and macrophase separation (——, ○), curves with Eq. (3), data from Fig. 7. (The dotted curve indicates where macrophase separation should start, at $f > f^*$ if the copolymer is replaced by a random copolymer [19].)

separation at solvent concentrations ϕ^* decreasing a bit with increasing f. The observed concentrations ϕ^* coincide with the model curve at low f, but are high at high f. We conclude from Figs. 6 and 8 that the model does qualitatively well in describing the transition from macrophases to microphases at f^*.

The kinetics of phase separation at $\phi < \phi^*$ are beyond the RPA model. They are described by models of the spinodal decomposition [23, 24].

The microphase separation of the copolymer and the copolymer blend with $f = 0.7$ in Fig. 5c, d is uncomplicated. The SAXS peaks that grow at ϕ^* remain at $\phi < \phi^*$ practically constant in position and size, until all solvent is removed ($\phi = 0.55 \rightarrow 0$ in Fig. 5c, $\phi = 0.50 \rightarrow 0$ in Fig. 5d). The corresponding curves in Fig. 7 end, therefore, at $\phi < \phi^*$ in a plateau $I/I_{max} = 1$. This indicates *stable microphases.*

The macrophase separation of the homopolymer blend in Fig. 5a is more involved. The decay curve is at its maximum intensity at ϕ^* and drops off again at $\phi < \phi^*$. The curve in Fig. 7 exhibits, therefore, a sharp maximum at ϕ^*. This indicates *instable macrophases*, as is illustrated schematically by Fig. 9. The decay curve at $\phi > \phi^*$, where the solution is still homogeneous, has the RPA shape ($q^* = 0$). This curve is intensified at ϕ^*, but it also develops a peak $q^* > 0$, due to a "critical slow-down" of diffusion at low q [23]. The peak describes the periodicity of the newly born "macrophase" morphology that is extremely fine at the start, not much coarser than the microphase morphology of the copolymer. However, at $\phi < \phi^*$, this morphology coarsens,

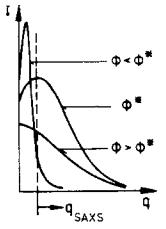

Fig. 9. Schematic structure factors for homogeneous ($\phi > \phi^*$) and demixed ($\phi < \phi^*$) solutions $A/B/L$, where phase separation produces unstable macrostructures, q_{SAXS}: q-range of SAXS

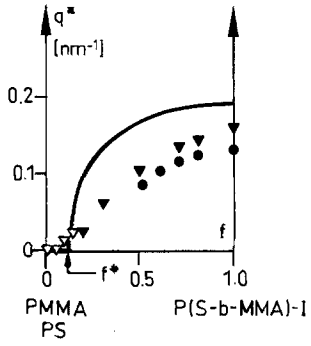

Fig. 10. Characteristic wave vector q^* of blends PMMA/PS/P(A-b-MMA)-I f^*: transition concentration, ●: SAXS, ▼: TEM, (symbols full: microphases, empty: macrophases)

and the peak moves, together with the whole SAXS curve, to lower q, out of the range of SAXS. The peak can then still be detected by light scattering [25] or TEM (in the form $\zeta = 2\pi/q^*$, see below).

The up and down of decay curves in Fig. 5a results when the phases coarsen so rapidly at $\phi < \phi^*$ that the peak travels immediately to $q < q_{SAXS}$. This situation, where the morphology consists of macrophases on the size scale of micrometers or more, corresponds, in the RPA model, to the prediction "$q^* = 0$".

The ternary blend PS/PMMA/P(S-b-MMA)-II with $f = 0.3$ in Fig. 5b represents a transition stage between the extremes. There is no peak in the SAXS curves, yet, the intensity does not drop off at $\phi < \phi^*$. The conclusion is that this blend starts forming a macrophase structure which, however, does not coarsen. This stage can be studied in more detail by TEM.

TEM pictures

The homopolymer blend PS/PMMA yielded, after film casting, an extremely coarse domain-matrix morphology, with spherical domains of PS, $\zeta \simeq 100\ \mu$m in diameter, in a matrix of PMMA. Evidently, structure coarsening proceeds rapidly in solution. Addition of the copolymer P(S-b-MMA)-II refined the morphologies, but the copolymer was needed in large quantities to produce microphase structures, as was shown in Fig. 6. The copolymer P(S-b-MMA)-II is not an efficient compatibilizer for the blend PS/PMMA.

Better suited is the copolymer P(S-b-MMA)-I, due to its longer chains. The ternary blends PS/PMMA/P(S-b-MMA)-I have the chain length ratio $\lambda = 0.19$, for which the low transition concentration $f^* = 0.11$ is predicted (Fig. 10). The morphologies in Fig. 11 prove that the copolymer P(S-b-MMA)-I is indeed a better compatibilizer. It had been shown in ref. [20] that lamellar microstructures are formed, in the ternary blends, at $f \geqq 0.20$. The important range of low f is now reconsidered.

Like the homopolymer blend, the ternary blend with $f = 0.05$ of copolymer has a rather coarse morphology. The average coarseness is $\zeta = 8\ \mu$m. Only part of a macrodomain and an interface is shown in Fig. 11a. This domain is full of inclusions. The blend with $f = 0.15$ in Fig. 11b has again a domain-matrix morphology, however, on a much finer scale, with domains that are comparable to the inclusions at $f = 0.05$. The blend with $f = 0.20$ in Fig. 11c has already a lamellar microstructure.The transition from domains to lamellae occurs thus at $f \simeq 0.20$, near the predicted f^* (Fig. 10). Figure 11b shows a transition stage that is equivalent to the transition stage observed in Fig. 5b.

The drastic reduction of morphology coarseness observed in Fig. 11 can be assigned to the compatibilizer effect of the copolymer (Fig. 2). It cannot be seen clearly that the copolymer chains are situated in the interfaces between phase domains. But heating the films to the liquid state did not provoke structure coarsening, which occurs inevitably in the homopolymer blend PMMA/PS [26]. The morphology on Fig. 11b is thus stabilized.

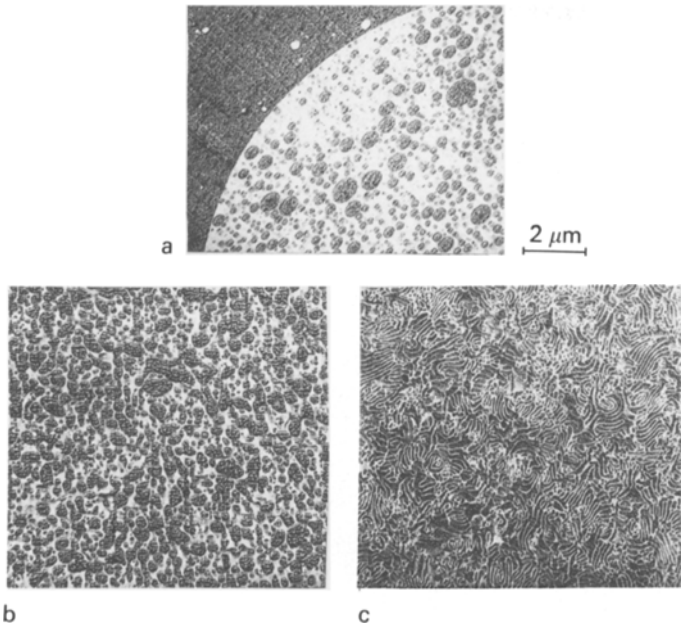

Fig. 11. TEM pictures of blends PMMA/PS/P(S-b-MMA)-I with a) $f = 0.05$, b) $f = 0.15$, c) $f = 0.20$

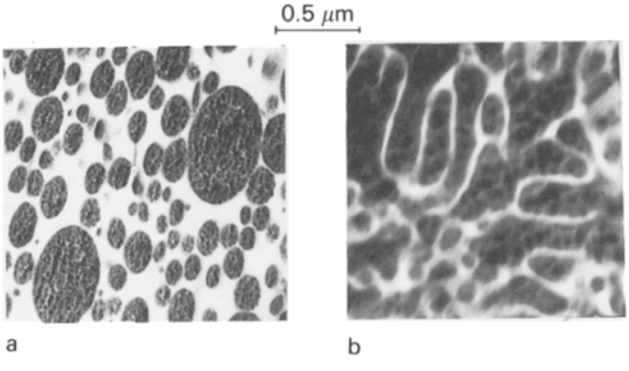

Fig. 12. Magnification of a) Fig. 11a, b) Fig. 11c

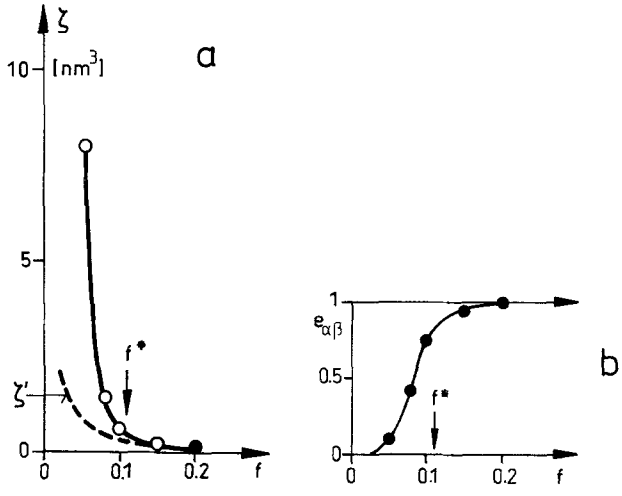

Fig. 13. a) Structure coarseness ζ of blends PMMA/PS/P(S-b-MMA)-I, ●: microphases, ○: macrophases, b) compatibilizer efficiency $e_{\alpha\beta}$ (Eq. (4))

But the compatibilization is at low f not as efficient as it could be. The inclusions in Fig. 11a are magnified in Fig. 12a. They are full of micelles (Fig. 2). The compatibilizer efficiency, i.e., the fraction of copolymer chains in interfaces, can be defined as

$$e_{\alpha\beta} = \zeta'/\zeta, \quad \zeta' = \zeta_{\alpha\beta}/f, \tag{4}$$

where ζ is the observed structure coarseness in a blend $A/B/\alpha\beta$, ζ' is the coarseness expected if all copolymer chains cover interfaces, and $\zeta_{\alpha\beta} = 45$ nm is the structure coarseness of the pure copolymer (Figs. 1 and 6).

Figure 13 shows ζ and the efficiency $e_{\alpha\beta}$ of the blends PS/PMMA/P(S-b-MMA)-I. The structure at $f = 0.05$ is ten times too coarse. The vast majority of the copolymer chains forms in this blend micelles. The efficiency $e_{\alpha\beta}$ is enhanced fast at higher f, but the blend with $f = 0.20$ still has micelles, as is seen in the magnification in Fig. 12b. Micelles disappear entirely only at $f \geqq 0.30$ [20].

In summary, the copolymer P(S-b-MMA)-I is a fairly good compatibilizer for the blend

PS/PMMA, but the efficiency at low f is still unsatisfactory, due to the formation of micelles.

(One can easily come to a better conclusion, due to an error that should be mentioned. Interfaces between the large macrodomains of coarse phase structures are sometimes hard to find in TEM pictures. Many of the TEM samples of the blend in Fig. 11a showed only inclusions, conveying the impression of a very fine morphology. Comparison of TEM pictures and light micrographs is necessary.)

Discussion

The transition concentration f^*, calculated for blends PS/PMMA/P(S-b-MMA) as a function of the chain volume ratio λ, is shown in Fig. 14. What the RPA model predicts, in qualitative terms, is whether the chains PS and PMMA of the homopolymers (range "macro") or the blocks S and MMA of the copolymer (range "micro") will demix earlier, during solvent evaporation. The good agreement of $f^*(\lambda)$ with the TEM data shown in Fig. 14 for $\lambda = 0.19$ (Fig. 10) and $\lambda = 0.50$ (Fig. 6) suggest that the phase structures of the dry blend films were indeed already pre-formed in solution. The SAXS curves in Fig. 5 support this view strongly.

But there is one important secondary effect, in blends in the vicinity of f^*. As macrophases of PS and PMMA are generated in these blends, on a fine scale, the copolymer P(S-b-MMA) is trapped inside these phases, where it forms micelles, or between them, where it partly covers the interfaces. The copolymer chains in micelles are probably lost for the compatibilizer effect which must rely on the chains in interfaces. These chains will, when the macrophases coarsen and the interfacial area is reduced, sooner or later form tightly packed monolayers in the interfaces. At this point, the coarsening should be stopped.

This mechanism of "delayed compatibilization" probably stabilizes the very fine macrophase morphologies of the blends in Figs. 5b and 11b.

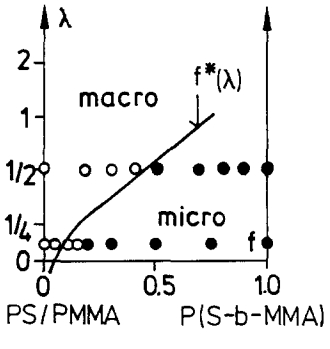

Fig. 14. Transition concentration $f^*(\lambda)$ for blends PMMA/PS/P(S-b-MMA) of different chain volume ratios λ, curve calculated, ●: microphases, ○: macrophases

Acknowledgement

We gratefully acknowledge financial support from the Bundesminister für Wirtschaft through the Arbeitsgemeinschaft Industrieller Forschungsvereinigungen (AIF). We should like to thank Dr. C. Johann and Dr. P. Kilz from Polymer Standards Service (Mainz, Germany) for preparing and characterizing the block copolymers.

References

1. Paul D (1978) In: Paul D, Newman S (eds) Polymer Blends. Academic Press, New York, Vol 2, Chap 12
2. Teyssie P, Fayt R, Jerome R (1988) Makromol Chem Makromol Symp 16:41
3. Fayt R, Jerome R, Teyssie P (1987) Polym Eng Sci 27:328
4. Xanthos M (1988) Polym Eng Sci 28:1392
5. Folkes MJ, Keller A (1973) In: Haward RN (ed) The Physics of Glassy Polymers. Applied Science Publishers, London, Chap 10
6. Thomas E, Alward D, Kinning D, Martin D, Handlin D, Fetters L (1986) Macromolecules 19:2197
7. Jiang M, Xie H (1991) Prog Polym Sci 16:977
8. Rigby D, Roe RJ (1984) Macromolecules 17:1778; (1986) 19:721
9. Kinning D, Thomas E (1989) J Chem Phys 90:5806; (1984) Macromolecules 17:1712
10. Kinning D, Winey K, Thomas E (1988) Macromolecules 21:3502
11. Leibler L, Orland H, Wheeler JC (1983) J Chem Phys 79:3550
12. Whitmore MD, Noolandi J (1985) Macromolecules 18:657
13. Inoue T, Soen T, Hashimoto T, Kawai H (1970) Macromolecules 3:87
14. Jiang M, Huang X, Yu T (1983) Polymer 24:1259
15. Jiang M, Cao X, Yu T (1986) Polymer 27:1917, 1923
16. Zin WC, Roe RJ (1984) Macromolecules 17:183, 189
17. Noolandi J, Hong KM (1982) Macromolecules 15:482
18. Xie H, Liu M, Jiang M, Yu T (1986) Polymer 27:1928
19. Löwenhaupt B, Hellmann GP (1991) Polymer 32:1065

20. Löwenhaupt B, Hellmann GP (1990) Colloid Polym Sci 268:885
21. Benoit H, Wu W, Benmouna M, Mozer B, Bauer B, Lapp A (1985) Macromolecules 18:986
22. Mori K, Tanaka T, Hashimoto T (1987) Macromolecules 20:381
23. Strobl GR (1985) Macromolecules 18:558
24. Furukawa H (1985) Adv Phys 34:703
25. Bates FS, Wiltzius P (1989) J Chem Phys 91:3258
26. Andradi LN, Hellmann GP (1993) Polymer 34:925

Received December 14, 1992;
accepted April 16, 1993

Authors' address:

Dr. G. P. Hellmann
Deutsches Kunststoff-Institut
Schloßgartenstraße 6
64289 Darmstadt, F.R.G.